Title

Surface coating determines the response of soybean plants to cadmium sulfide quantum dots (vol 14C, 100151, 2019)

Authors

Majumdar, Sanghamitra
Ma, Chuanxin
Villani, Marco
et al.

Publication Date

2021

NanoImpact 14 (2019) 100151

Contents lists available at ScienceDirect

NanoImpact

journal homepage: www.elsevier.com/locate/nanoimpact

Surface coating determines the response of soybean plants to cadmium sulfide quantum dots

Sanghamitra Majumdar[a,b,c], Chuanxin Ma[a], Marco Villani[e], Nubia Zuverza-Mena[a], Luca Pagano[d], Yuxiong Huang[b,c], Andrea Zappettini[e], Arturo A. Keller[b,c], Nelson Marmiroli[d], Om Parkash Dhankher[f], Jason C. White[a,*]

[a] Department of Analytical Chemistry, The Connecticut Agricultural Experiment Station, New Haven, CT 06504, United States
[b] University of California, Center for Environmental Implications of Nanotechnology, Santa Barbara, CA 93106, United States
[c] Bren School of Environmental Science and Management, University of California, Santa Barbara, CA 93106, United States
[d] Department of Chemistry, Life Sciences and Environmental Sustainability, University of Parma, Parma 43124, Italy
[e] Institute of Materials for Electronics and Magnetism (IMEM-CNR), Parma, Italy
[f] Stockbridge School of Agriculture, University of Massachusetts, Amherst, MA 01003, United States

ARTICLE INFO

Keywords:
Quantum dots
Soybean
Surface coating
Oxidative stress
Localization
Lignification

ABSTRACT

Quantum dots (QDs) are used in an array of applications from electronic devices to medicine, leading to environmental release and accumulation in landfills and agricultural soils. However, their effects on plants have been least studied among other engineered nanomaterials. In the current study, soybean seedlings were exposed to 50–200 mg/L cadmium sulfide quantum dots (CdS-QDs) to elucidate their bioaccumulation and biological response in comparison to Cd^{2+} ions and bulk-CdS. To understand the role of surface coatings on QD stability, uptake, translocation, subcellular localization and cellular response, bare CdS-QDs were capped with ligands varying in polarity and surface charge. Four common ligands, including trioctylphosphine oxide, polyvinylpyrrolidone, mercaptoacetic acid, and glycine were used to synthesize QD-TOPO, QD-PVP, QD-MAA, and QD-GLY, respectively. In aqueous suspension, QD-MAA particles were most stable, maintaining their size at 332 nm with least Cd^{2+} dissolution (9%) after 14 d, whereas QD-TOPO formed large aggregates of size 3861 nm with 27% Cd^{2+} dissolution. Upon exposure to 100 mg/L bare and coated CdS-QDs in vermiculite for 14 d, soybean roots accumulated Cd, ranging from 568 (QD-MAA) to 1010 (QD-PVP) μg/g tissue dry weight (DW); statistically equivalent to bulk-CdS treatment (639 μg/g DW). In the roots, Cd from $CdCl_2$, bulk- CdS, QD-MAA and QD-GLY accumulated primarily in the cell wall (~40–55%) followed by organelles (28–40%), suggesting apoplastic pathway; whereas in QD-TOPO, dissolved Cd^{2+} ions accumulated mainly in the membranes. The exception was QD-PVP, which sequestered Cd mainly in the organelles (49%) in roots, potentially *via* symplastic pathway and translocated to shoots, resulting in reduced leaf biomass. Results suggested that peroxidases play the predominant role in quenching the oxidative stress caused by CdS-QD exposure. At the highest CdS-QD treatment (200 mg/L), root lignification allowed the plants to restrict Cd accumulation, except in QD-PVP, where lignification was reduced by 21% leading to higher Cd content in shoots. Increased amino acid content in the leaves was noted as a stress tolerance mechanism by the plants exposed to 200 mg/L QD treatments. This study highlights the significant influence that surface coating exerts on QDs fate and effects in a planted system.

1. Introduction

A wide range of engineered nanomaterials (ENMs) with unique and tunable properties have been increasingly incorporated in a large array of industrial and consumer products. The burgeoning ENM production without effective regulation strategies for use and disposal have raised concerns about their release and subsequent accumulation in different environmental compartments, predominantly in soils and sediments (Garner et al., 2017; Wang and Nowack, 2018). Quantum dots (QDs) are one of the major classes of ENMs with unique electronic properties, high photostability, bright fluorophores, and size-tunable narrow fluorescence emission bands (Jin et al., 2011; Efros et al., 2018). Most

* Corresponding author at: Department of Analytical Chemistry, The Connecticut Agricultural Experiment Station, 123 Huntington Street, P.O. Box 1106, New Haven, CT 06504-1106, United States.
E-mail address: Jason.White@ct.gov (J.C. White).

https://doi.org/10.1016/j.impact.2019.100151
Received 9 November 2018; Received in revised form 10 February 2019; Accepted 11 March 2019
Available online 13 March 2019

QDs have a chalcogenide II–IV, IV–VI, or III–V semiconductor core (CdX; X = S, Se, Te), and an outer shell to improve photoluminescence quantum yield, stability, and to block surface deficiencies to prevent leaching of the core metal ion (Mo et al., 2017). The shells may be further coated with application-targeted ligands to optimize properties and performance (Boles et al., 2016).

Trioctylphosphine and trioctylphosphine oxide (TOP/TOPO) have been used as the standard capping agents for organometallic-type synthetic routes of QDs providing hydrophobic surface to CdS, CdSe or CdTe QDs (Mo et al., 2017). Ligand exchange methods are used to modify the QD surface with water soluble and biocompatible ligands like thiol groups, amino acids, polyethylene glycol (Green, 2010) and stabilizing agents like polyvinylpyrrolidone (PVP) (Shahi et al., 2017). The most prominent applications of QDs are in the field of medicine (drug delivery, imaging, and diagnostics) (Abbasi et al., 2016), biosensing (Petryayeva et al., 2013; Altintas et al., 2017) and electronics (quantum computing, light emitting diodes for displays, lighting, and photovoltaics) (Xie et al., 2016; Owen and Brus, 2017). Dynamic probabilistic material flow analysis models have estimated that a major fraction (> 70%) of QDs are used in electronic devices which could be released to the environment during recycling, and ~25% of that used in medicine ends up in the incineration waste, which eventually leads to accumulation in landfills and sludge treated soils at ng/kg to μg/kg levels (Wang and Nowack, 2018).

Surface modifications play an important role in determining ENMs' fate in environmental matrices and interaction with biota (Oh et al., 2016). Additionally, organic acids, amino acids, proteins, and inorganic oxyanions present in these matrices may participate in stabilization and ligand exchange reactions at the nanoparticle-matrix interface (Mudunkotuwa and Grassian, 2015). The electrostatic properties tend to control colloidal stability in different matrices, depending on the dominant charge of the media and the counter-ions in the diffuse region of the core particle (Boles et al., 2016; Domingos et al., 2013). Wang et al. showed that the transport of CdSe/ZnS or CdSe/CdZnS QDs in sand is primarily governed by the surface charge of the particle rather than the molecular weight of the ligand or the overall particle size (Wang et al., 2013). Surface modified ENMs with negative zeta (ζ) potential have been shown to be more mobile in sand compared to positively charged or neutral particles (Wang et al., 2013; Zhang et al., 2018), thereby increasing bioavailability and *in planta* translocation to aerial tissues (Judy et al., 2012; Zhu et al., 2012; Spielman-Sun et al., 2017; Ashfaq et al., 2017; Al-Salim et al., 2011; Koo et al., 2015). It is important to understand the mechanisms controlling ENM bioavailability, localization, and accumulation, as well as associated impacts on plant and soil health, as influenced by surface coating. Several researchers have investigated the uptake of differentially coated QDs (Koo et al., 2015; Li et al., 2018), metal-based (Zhang et al., 2018; Judy et al., 2012; Zhu et al., 2012; Spielman-Sun et al., 2017; Li et al., 2016), and carbon-based (Ashfaq et al., 2017) nanomaterials by plants. Among ENMs, QDs are the least studied in agricultural crops, thus demanding immediate attention. A few publications have used fluorescence detection of QDs in plants to track their transport *in vivo* (Al-Salim et al., 2011; Koo et al., 2015; Li et al., 2018; Hu et al., 2010); however, these studies failed to address biological responses. In addition, there is little understanding of how ENM properties change over time in the exposure media, influencing the mechanisms controlling uptake or toxicity. Thus, there is limited understanding of QD uptake by plants, although it is clear that particle surface properties will be an important factor guiding these interactions. Positively charged QDs will likely adhere to the roots, being retained by the epidermal cells due to electrostatic binding with the negatively charged root surface (Spielman-Sun et al., 2017; Li et al., 2018). Conversely, negatively charged particles coated with carboxyl groups have been shown to be effectively transported to leaves (Li et al., 2018; Whiteside et al., 2009). Some studies have also suggested that species-specific rhizosphere biochemistry mediates QD uptake and translocation, which may partially explain the inconsistent reports on particle-plant interactions in the literature (Judy et al., 2012; Zhu et al., 2012). Furthermore, (Koo et al., 2015) trophic transfer of CdSe QDs coated with poly(acrylic acid-ethylene glycol) and polyethyleneimine from *Arabidopsis thaliana* leaves to an herbivorous species, the cabbage looper (*Trichoplusia ni*) has also been reported (Koo et al., 2015). In another study, carboxylated CdTe QDs were shown to biomagnify in protozoans (ciliates) that had been fed on *Escherichia coli* exposed to QDs for 1 h (Gupta et al., 2017).

In the current study, we investigated the response of soybean plants upon exposure to CdS-QDs, bulk-CdS and Cd^{2+} ions. Effects on the biological processes in response to CdS-QDs with different surface coatings, varying in charge and composition were also tested. Toxicity assessment studies were based on oxidative stress assays and metabolite levels in the plant tissues. Cadmium bioavailability, bioaccumulation, and sequestration in cellular compartments of the soybean tissues were determined as a function of surface coating. The findings of this study provide important information on the interaction of QDs with terrestrial plant species that can be used to establish an accurate assessment of both exposure and risk in agricultural systems.

2. Experimental

2.1. Chemicals

Cadmium acetate ($Cd(CH_3COO)_2$, 99%), *N,N*-dimethylformamide (DMF, 99%) and thiourea (99.5%) were purchased from VWR International (Radnor, Pennsylvania, USA). Cadmium chloride ($CdCl_2$), equivalent bulk CdS, and the capping agents, including TOPO (99%), PVP (10,000 g/mol), mercaptoacetic acid (MAA, 99%), glycine (GLY, 99%), and the reagents used for the biochemical assays were purchased from Sigma Aldrich (Saint Louis, MO, USA). All reagents were used without further purification.

2.2. Nanomaterial synthesis and characterization

Gram-scale CdS-QDs were synthesized by optimizing a previously reported procedure. (Calestani et al., 2014; Villani et al., 2012) Four different capping agents (TOPO, PVP, MAA, GLY) varying in constituent functional groups, surface charge, and polarity were used to functionalize the bare CdS-QDs (Supplementary material Table S1). Henceforth, the bare CdS-QDs will be referred as QD-Bare and the coated QDs will be referred as QD-TOPO, QD-PVP, QD-MAA, and QD-GLY representing their respective ligand groups. The synthesis procedure of the CdS-QDs is described in Supplementary material Method S1. X-ray diffraction (XRD) of the CdS-QDs was performed using an ARL-X'Tra device (Thermo Fisher Scientific, MA, USA) using the Cu Kα source, in a Θ-Θ Bragg-Brentano geometry (10^{-4} degree accuracy). To evaluate the functionalization of the CdS-QDs, attenuated total reflectance-Fourier transform infrared spectroscopy (ATR-FTIR) was performed using a Thermo FTIR (Nicolet iS10) at room temperature (23.5 ± 0.4 °C) in the wave number range from 4000 to 400 cm^{-1}.

2.3. Characterization and stability of the quantum dots

For characterization purposes, QD suspensions were prepared in Milli-Q water (MQW) at a concentration of 100 mg/L. Pulsed probe sonication at 40% amplitude for 2 min (Fisher Scientific Model 505 sonic dismembrator, Waltham, MA, USA) was used to minimize aggregation. The average size (hydrodynamic diameter) and ζ-potential (Zetasizer Nano ZS, Malvern Instruments, Worcestershire, United Kingdom) of the suspensions were measured in triplicates at different time points, t = 0 h, 6 h, 24 h, 48 h, 7 d and 14 d.

To study the dissolution kinetics of the CdS-QDs for 14 d, samples were collected from the aqueous suspensions at t = 0 h, 6 h, 24 h, 48 h, 7 d and 14 d. Percent dissolution was calculated with respect to the total Cd content measured in the aliquots of the respective suspensions.

Thus, at each time point, 8 mL solution from each CdS-QD suspension was divided into two portions; the first aliquot was used to quantify the total Cd content, and the second portion was passed through Amicon 3KDa centrifugal filters for 2 h at 3000 rpm in an Eppendorf 5810 centrifuge to quantify the dissolved Cd^{2+} fraction. The aliquots from each CdS-QDs were weighed and acidified with HNO_3; the final solutions were diluted to 5% HNO_3. The acidified solutions were analyzed for Cd and S content by inductively coupled plasma-optical emission spectrometry (ICP-OES, iCAP 6500, Thermo Fisher Scientific, Waltham, MA) using Yttrium-89 as internal standard.

2.4. Plant growth and exposure conditions

Soybean seeds (*Tohya* variety) were purchased from Johnny's Selected Seeds (Albion, ME, USA) and were surface sterilized with 1% sodium hypochlorite solution, rinsed thoroughly and soaked in MQW for 24 h. The seeds were germinated in vermiculite for 11 d until the appearance of the first true leaf and seedlings without any apparent tissue damage and similar lengths were transplanted to 40 mL (6 g) of vermiculite in 50 mL centrifuge tubes amended with suspensions of QD-Bare, QD-TOPO, QD-PVP, QD-MAA, or QD-GLY at 50, 100 and 200 mg QD per L vermiculite. Additional treatments were established for vermiculite control containing MQW only, an ionic treatment at 10 mg/L $CdCl_2$, and a bulk equivalent at 100 mg/L CdS. The concentration of the ionic treatment was established at 10% dissolution of the QDs based on preliminary results (Fig. 2C). The bulk-CdS was selected to enable comparison of particles with similar chemical composition, but lacking the unique properties at nanoscale. The bulk-CdS suspension was established at 100 mg/L, similar to the middle concentration of the CdS-QDs. All treatments were performed in quadruplicate. The plants were grown for 14 d at 24 °C at a relative humidity of 30%, and under a 16 h photoperiod (light intensity 120 $\mu M\, m^{-2} s^{-1}$ photosynthetic photon flux). The plants were watered as needed and were grown without any additional nutrients. The details on the preparation of suspension/solution and exposure in vermiculite is provided in Method S2.

2.5. Cadmium and nutrient accumulation and distribution

After 14 d of exposure, all plants were harvested for determination of physiological parameters. For elemental analyses, the plants were rinsed lightly with MQW inside the tube to remove vermiculite adhered to the root surface, followed by three alternating rinses outside the tube with 0.01 M HNO_3 and MQW to remove any residual nanoparticles loosely bound to the surface. The plants were blotted dry with paper towel, and the length of the roots and shoots were measured. The plants were then separated into roots, stems (including cotyledons) and leaves. The fresh weight of each tissue was measured and dried in an oven at 70 °C for 72 h. The vermiculite in each tube was also dried at 70 °C for 96 h and was retained for determination of Cd and inorganic ions.

Oven dried plant samples were digested in 2:1 HNO_3:H_2O_2 on a SCP Science DigiPREP hot block digestion system at 115 °C for 60 min. A fraction (~0.5 g) of the oven dried vermiculite samples was digested in concentrated HNO_3 at 115 °C for 60 min. The digests were diluted to 50 mL. A reference material (SRM 1573a tomato leaves) was processed in each digestion set and 98% recovery of Cd was achieved. The digested vermiculite and root samples were filtered and analyzed by ICP-OES; stem and leaf samples were analyzed by ICP-mass spectrometry (Agilent ICP-MS 7500, Agilent Technologies, Santa Clara, CA, USA) for Cd. The macronutrients (Ca, Mg, S, K, P) and micronutrients (Cu, Fe, Mn, Mo, Na, Ni, Zn, B) in the plant tissues were analyzed by ICP-OES. For all ICP analyses, analytical and matrix blanks were introduced in every sequence, and a calibration verification standard was run every 12 samples.

2.6. Subcellular localization of cadmium

Fresh root and shoot tissues from plants exposed to 0, 200 mg/L of CdS-QDs, 10 mg/L $CdCl_2$, and 100 mg/L bulk-CdS were ground in a mortar and pestle using liquid nitrogen. Approximately 0.4 g of tissues were extracted in 4 mL of 50 mM Tris HCL (pH 7.5) containing 250 mM sucrose and 1 mM dithioerythritol (DTE) (*Buffer A*) (Fourati et al., 2016). Cadmium distribution in four different cellular sub-fractions was analyzed; the insoluble fraction containing cell wall and debris (I), organelle fraction including the chloroplasts, mitochondria *etc* (Hernández et al. (1998)). (II), the cell membrane fraction (III), and the soluble fraction containing vacuoles and the cytosol (IV). The extracts were centrifuged at 500 $\times g$ for 30 s using an Eppendorf 5810R centrifuge. The pellet (fraction I) was collected and the supernatant was centrifuged at 10,000 $\times g$ for 30 min using a Beckman Coulter Optima MAX-130K Ultracentrifuge to precipitate fraction II. Finally, the supernatant was centrifuged at 100,000 $\times g$ for 30 min to collect fraction III in the pellet, and the obtained supernatant was retained as fraction IV. All steps were carried out at 4 °C. The obtained fractions were lyophilized for 24 h in a freeze dryer (Labconco Co., Kansas City, MO) and digested using 2:1 HNO_3:H_2O_2. Due to low weight of individual fractions, the replicates were pooled into a single composite, and therefore, statistical analysis could not be performed. Fraction I was diluted to 35 mL and II–IV were diluted to 10 mL; all fractions were analyzed using ICP-MS.

2.7. Primary and secondary metabolite content

Primary metabolites including total soluble protein, amino acids, and photosynthetic pigments were quantified in the leaves from soybean plants exposed to control, 50–200 mg/L CdS-QDs, 10 mg/L $CdCl_2$, and 100 mg/L bulk-CdS. The photosynthetic pigments including carotenoid and chlorophyll *a* and *b* were determined spectrophotometrically in the 80% acetone extracts of first true leaves (Ni et al., 2008. Total soluble protein and amino acid content were determined in the second true leaves from the control and treated plants (Bradford, 1976; Huang et al., 2018). Secondary metabolites including the total phenolic content in the leaves and total lignin content in the roots were also determined in the plants (Zheng and Wang, 2001; Moreira-Vilar et al., 2014). Detailed analytical methods for primary and secondary metabolite determination in soybean tissues are provided in Methods S3 and S4.

2.8. Antioxidant enzymes assays

For determining the activities of the major oxidative stress enzymes in soybean leaves, the second true leaves were extracted in 50 mM phosphate buffer (pH 7.4) containing 1 mM EDTA, 1% (w/v) PVP, and 0.5% (v/v) Triton X-100. The extracts were centrifuged at 10,000 $\times g$ for 20 min at 4 °C in an Eppendorf 5417R centrifuge. The supernatants were analyzed for superoxide dismutase (SOD), catalase (CAT), ascorbate peroxidase (APX), and guaiacol peroxidase (GPX) according to Majumdar et al. with minor modifications (Majumdar et al., 2014). The SOD activity was expressed as SOD units per mg of protein. The CAT, APX and GPX activities were expressed as mg H_2O_2 degraded min^{-1} $(mg\ protein)^{-1}$.

2.9. Statistical analysis

The results are expressed as mean ± standard error (SE) ($n = 4$) unless otherwise noted. A one-way ANOVA test followed by Tukey's multiple comparison test was performed to determine significant difference at $p \leq 0.05$ between different CdS-QDs at 100 mg/L and compared to control, ionic and bulk-CdS treatments. A two-way ANOVA test was performed to determine the effect of coating and duration on the

CdS-QD stability, and the effect of the coating, treatment concentration and their interaction on plant parameters. The IBM SPSS Statistics version 24 package was used for all statistical analysis. For amino acid analysis, the data were processed with Agilent MassHunter Workstation Software Quantitative Analysis (Version B.07.01/Build 7.1.524.0). The statistical analysis including principal component analysis (PCA), one-way ANOVA, and hierarchical clustering analysis for the amino acids were performed using Metaboanalyst 4.0.

3. Results and discussion

3.1. Characterization of the CdS-QDs

The four ligands used in this study, TOPO, PVP, MAA, and GLY have representative functional groups known to efficiently stabilize QDs (Mo et al., 2017; Green, 2010), and yield materials with a range of surface charge and polarity (Table S1). The powder XRD patterns clearly suggests that all CdS-QD samples can be indexed as either cubic or hexagonal, or a mixture of the two phases (Fig. S1). Given the peak broadening from defects and size confinement, the dimension of the grain size was estimated from the full width at half maximum of the main peak within the Scherrer approximation. Considering the narrowest peak, which corresponds to the largest grain size, the CdS-QD mean dimensions can be safely assumed to be smaller than 8 nm, which is comparable to QDs in existing literature (Koo et al., 2015).

The coatings of the bare CdS-QDs with TOPO, PVP, MAA and GLY were confirmed by FTIR analysis (Fig. 1A) and the scheme of the ligand attachment to the core, as interpreted from the spectra is shown in Fig. 1B. The FTIR spectrum of QD-Bare (Fig. 1A) shows a broad peak from 3185 to 3320 cm^{-1} representing OH stretching vibrations, and complex deformations centered at 1629, 1538,1409, 1006, and 665 cm^{-1}, which represent C═O asymmetric stretching, NH bending, C═O symmetric stretching, C—H bending, and CdS-stretching, respectively on CdS-QD surface (Kotkata et al., 2009; Javed et al., 2016). The FTIR of QD-TOPO reveals a characteristic peak corresponding to $-CH_2$ stretching at 2931 cm^{-1} present in TOPO molecule (Young et al., 2008), and a broad peak for —OH stretching at 3316 cm^{-1}. The P═O stretching vibration peak wavenumber in the QD-TOPO was broadened to include several bands centered at 1061 and 1097 cm^{-1}, which was shifted from the peak of TOPO molecule alone at ~1150 cm^{-1} (data not shown). This lowering and broadening is in agreement with Young et al. and confirms coordination through the donation of lone pair of electrons from the O atom in the phosphine oxide to Cd (Fig. 1B), as previously reported using *ab initio* calculations (Green, 2010; Young et al., 2008). The QD-PVP spectrum also shows broad OH stretching vibration centered at 3261 cm^{-1}, demonstrating the affinity of the particles to atmospheric moisture (Fig. 1A). There is also an NH stretch evident from the characteristic peak at 1563 cm^{-1}. The peak at 1399 cm^{-1} signifies CH bend vibrations in the PVP structure, also visible in QD-TOPO. A strong characteristic peak for C═O present in PVP alone at 1680 cm^{-1} (data not shown) was shifted to a smaller peak at 1655 cm^{-1}, which could be due to coordination with S from the CdS surface, as indicated from the S═O stretching vibration at 1343 cm^{-1}. The characteristic peak for a C—N stretch that was present in PVP alone at 1285 cm^{-1} was also shifted in the QD-PVP spectrum. A broad peak from 1950 to 2150 cm^{-1} in the QD-PVP, not originally present in the PVP itself, was attributed to an asymmetrical N-C-S stretching vibration. This suggested that PVP coordinated *via* O or C (replacing O) to the S of the CdS-QDs (Fig. 1B). The OH stretching vibration from the carboxyl group is also apparent in the spectrum of QD-MAA at 3173 cm^{-1} (Fig. 1A). The peaks at 1545, 1390, and 1219 cm^{-1} indicate the presence of mercaptoacetate ions (Young et al., 2006). The absence of the characteristic stretching vibration bands of SH at 2535 to 2600 cm^{-1} and C═O from carboxylic acid at 1700 to 1730 cm^{-1}, implies that MAA coordinates with CdS-QDs through both mercapto- and carboxyl ends (Fig. 1B). Previous studies also suggest that thiol group attaches *via* the deprotonated S atom to metal based nanoparticles (Green, 2010; Li et al., 2016; Gaceur et al., 2012) or through the carboxyl end (Xia et al., 2016). The striking feature of strong H bonding due to —OH and *ν*(NH) stretching was observed in the region of 3276 cm^{-1} in the QD-GLY spectrum. The absence of peaks representing carboxylic groups and the presence of the characteristic peak for —NH bend (1559 cm^{-1}) and alkyl C—N (1042 and 1098 cm^{-1}) stretching vibrations in amines in the fingerprint region of QD-GLY spectrum suggests coordination through O to the QD surface (Fig. 1). Similar preservation of the $-NH_2$ group was also observed in the synthesis of

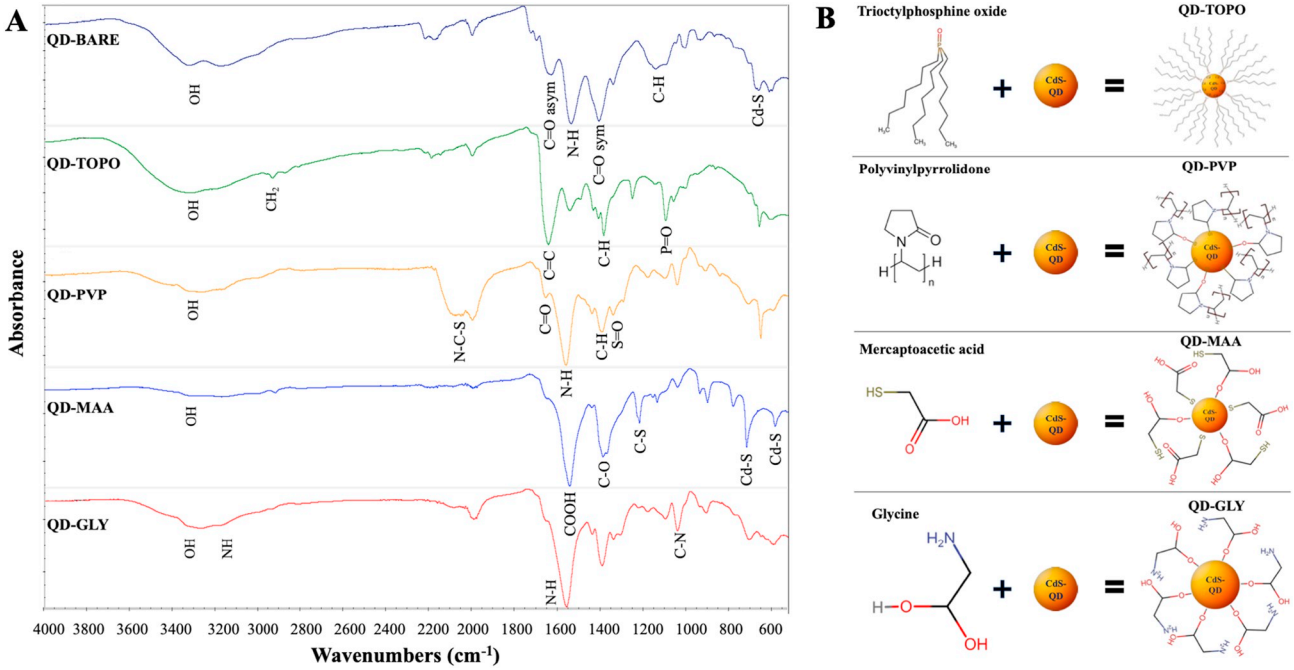

Fig. 1. (A) FTIR spectra of the bare and coated CdS-QDs; (B) schematic representation of surface coating of CdS-QDs with trioctylphosphine oxide (TOPO), polyvinylpyrrolidone (PVP), mercaptoacetic acid (MAA) and glycine (GLY) based on FTIR results.

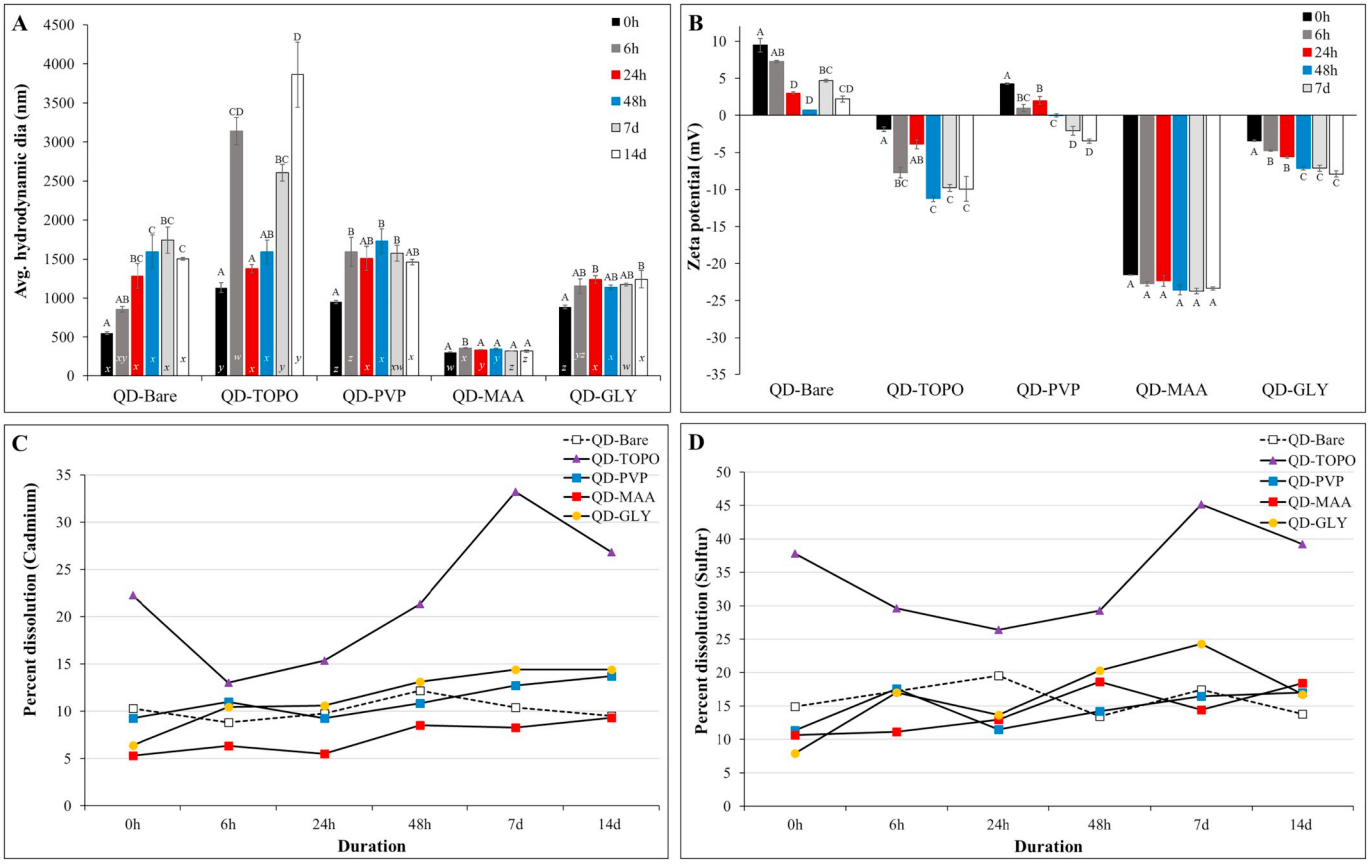

Fig. 2. Characteristics of 100 mg/L CdS-QD suspensions for 14 d. (A) Average hydrodynamic diameter (nm), (B) zeta potential (mV), (C) percent dissolution of cadmium, and (D) percent dissolution of sulfur. Values are expressed as Mean ± SE. The bars with different uppercase letters in (A) and (B) represent significant differences within same CdS-QD type, and different lowercase letters in (A) represent significant differences between different CdS-QDs at each time point, as determined by one-way ANOVA and Tukey's multiple comparison test ($p \leq 0.05$).

oleylamine FePt nanoparticles (Shukla et al., 2003). The FTIR spectra of the functionalized CdS-QDs in solid phase thus provides important information on the availability of functional groups that mediate stability in the suspension as explained further, which may play decisive role during their interaction with biota.

3.2. Characterization of QD suspensions

The hydrodynamic diameter of the CdS-QDs measured by DLS reflect the size of aggregates and the influence of organic and solvation layers on the effective size of the CdS-QDs, and not the primary particle size. Immediately after preparing the suspensions, at $t = 0$ h, the average hydrodynamic diameter of QD-Bare (550 ± 16 nm) was significantly smaller ($p \leq 0.001$) than QDs coated with TOPO (1134 ± 62 nm), PVP (950 ± 20 nm), and GLY (884 ± 24 nm), but significantly larger ($p = 0.002$) than QD-MAA (306 ± 2 nm) (Fig. 2A). The size of QD-MAA in suspension was stable throughout 14 d unlike other CdS-QDs, which could be due to the availability of the carboxyl and hydroxyl groups on the QD-MAA surface (Fig. 1) allowing stable hydrogen bonds with water molecules. After 24 h, QD-MAA measured 337 ± 4 nm, which was significantly smaller than QD-Bare (1282 ± 159 nm), QD-TOPO (1378 ± 53 nm), QD-PVP (1510 ± 155 nm), and QD-GLY (1153 ± 94 nm). The QD-GLY in suspension became stable in 6 h, however the hydrodynamic diameter of the particles were significantly larger than QD-MAA. The coordination of MAA and GLY to CdS-QD through the carboxyl O, as determined from FTIR spectra, imparts exceptional colloidal stability to the respective QDs in MQW for 14 d by exposing hydrophilic functional groups (Fig. 1). QD-Bare and QD-PVP in suspension stabilized after 24 h except QD-TOPO, which continued to aggregate to 3861 ± 416 nm in 14 d (Fig. 2A). The coating of the QDs with TOPO exposed the long hydrophobic alkyl chains (Fig. 1), thereby destabilizing the particles in the colloidal suspension leading to formation of large aggregates (Fig. 2A).

The ζ-potential of the CdS-QD suspensions at $t = 0$ h were 9.5 ± 0.95 (QD-Bare), −1.9 ± 0.3 (QD-TOPO), 4.3 ± 0.1 (QD-PVP), −21.5 ± 0.0 (QD-MAA), and − 3.4 ± 0.1 (QD-GLY) mV (Fig. 2B). The stability of QD-MAA in the suspension is also evident from high negative zeta potential for 14 d (−22.87 ± 2.05 mV). This is in accordance with Xia et al. (2016), suggesting that -SH from MAA coated TiO_2 nanoparticles reacts with hydroxyl ions in solution, producing a negatively charged coating of S^- ions around the colloid leading to electrostatic repulsion (Xia et al., 2016). The ζ-potential of all the other CdS-QD suspensions decreased significantly with time and ranged between ± 0 to 10 mV, which explains their unstable nature.

A 14 d dissolution kinetic study in aqueous solution showed that Cd^{2+} was released from all the QDs, with the order being QD-MAA < QD-Bare < QD-PVP < QD-GLY < QD-TOPO (Fig. 2C). A study by Domingos et al. (2013) showed increased Cd^{2+} release from core/shell CdTe/CdS carboxyl-terminated QDs coated with citric acid at a wide range of pH; however, glycine coating did not affect the QD dissolution at pH 6.0, but decreased dissolution at pH 8.5 by destabilizing the surface charge on the QD (Domingos et al., 2009). The dissolution of Cd^{2+} from 1 h to 14 d in QD-MAA, QD-PVP, QD-GLY, and QD-TOPO suspensions increased from 5.3 to 9.3%, 9.2 to 13.7%, 6.4 to 14.4% and 22.3 to 33.2%, respectively. QD-TOPO released significantly more Cd^{2+} ions at all the time points compared to other CdS-QDs, except at 6 h due to large variance in the QD-TOPO data on that day. The highest percent dissolution of Cd from QD-TOPO could also be due to the lowest bond dissociation energy of Cd—O (Luo and Kerr, 2018), compared to other CdS-QDs, as TOPO attaches to CdS through the

coordination of O atom from P═O of TOPO to Cd (Fig. 1). The dissolution of S^{2-} ions was higher than Cd^{2+} ions, but showed the same overall kinetic trend (QD-MAA (10.6–18.6%) < QD-PVP (11.4–17.6%) < QD-Bare (13.4–19.5%) < QD-GLY (7.9–24.3%) < QD-TOPO (26.4–45.1%) (Fig. 2D). Higher S^{2-} dissolution suggests that the ligands were mostly attached to Cd; a similar observation was made in CdSe core QDs functionalized with polyethelenimine or an amphiphilic polymer coated with amine or carboxylic acid (Lee et al., 2016). According to FTIR results, PVP was attached to the S atoms in the CdS-QDs (Fig. 1), thereby justifying lower release of S^{2-} compared to QD-Bare. It is to note that the dissolution study guided our selection of the concentration for $CdCl_2$ treatment for the plant experiments at 10 mg/L, as the average dissolution of Cd^{2+} from the CdS-QDs after 1 h was 10.7% (Fig. 2C). A two-way ANOVA of our results suggests that both coating type and duration of the experiment affected the Cd^{2+} dissolution, calculated as a fraction of total Cd in the suspension. Two way ANOVA suggested that there was a significant interaction between the effects of coating and duration on the size ($F(20, 90) = 16.0$, $p \leq 0.001$), ζ-potential ($F(20, 90) = 10.7$, $p \leq 0.001$), and dissolution ($F(20, 90) = 4.8$, $p \leq 0.001$) of the CdS-QDs.

3.3. Impact of CdS-QDs on plant growth and physiology

Little overt toxicity symptoms were observed in soybean exposed to 50–,100, and 200 mg/L CdS-QDs, 100 mg/L bulk-CdS and 10 mg/L $CdCl_2$, as compared to the control (Fig. S2). A statistically significant reduction in leaf and total plant biomass was only noted for the plants treated with 200 mg/L QD-PVP (Fig. S2B). Specifically, the total biomass of the plants exposed to 200 mg/L QD-PVP was significantly decreased ($p = 0.04$) to 1.94 ± 0.96 g from 2.74 ± 0.18 g for the control plants. Although the root biomass and primary root length was not significantly affected by Cd treatments, browning of the primary roots and reduction in the secondary root development was observed in all the plants exposed to 200 mg/L CdS-QDs (Fig. S3). It has been previously reported in rice (*Oryza sativa* L.) that Cd at 100 μM induces severe damage to the lateral root primordium and the quiescent center (Ronzan et al., 2018). An exposure of 50 to 100 μM $CdCl_2$ to soybean and peas (*Pisum sativum*) was shown to induce lignin formation, leading to cell wall stiffening and reduced root growth (Finger-Teixeira et al., 2010). In response to CdS-QDs in our study, the soybean roots restricted lateral root development as a stress avoidance mechanism in response to the high concentration of CdS-QDs. Similar to our observations, Rodriguez-Serrano et al. showed that in peas, Cd treatment resulted in browning of the roots and lateral root thickening, which was attributed to an increase in the number of cortex cells, and modification of the stele morphology, resulting in smaller xylem vessels and less developed phloem cells (Rodrígues-Serrano et al., 2006).

3.4. Cadmium accumulation in soybean tissues

Fourteen-day exposure to 100 mg/L CdS-QD resulted in accumulation of 774 ± 63 (QD-Bare), 755 ± 129 (QD-TOPO), 1010 ± 255 (QD-PVP), 568 ± 97 (QD-MAA) and 708 ± 4 (QD-GLY) μg Cd/g tissue dry weight (DW) in the soybean roots (Fig. 3A). The roots from the plants exposed to 100 mg/L bulk-CdS treatment also accumulated at similar levels as the CdS-QDs (639 ± 109 μg/g DW). Except QD-MAA and QD-GLY, root Cd content in 100 mg/L CdS-QDs was significantly higher than $CdCl_2$ treatment (165 ± 47 μg/g DW) (Fig. 3A). Although all the roots exposed to CdS-QDs showed a dose-dependent trend in Cd content, a statistically significant increase with increasing exposure concentration was only observed in QD-TOPO, QD-PVP at 100 and 200 mg/L and in QD-MAA at 200 mg/L, compared to their respective 50 mg/L treatments. There was no significant difference in root Cd content between different CdS-QD coatings at similar exposure concentrations. A two-way ANOVA suggested that there was no significant interaction between the effects of coating and concentration of CdS-QDs on Cd accumulation in the roots, $F(8, 44) = 1.6$, $p = 0.158$. Although coating did not have significant effect on the Cd content in roots $F(4, 44) = 1.062$, $p \leq 0.387$), the root Cd accumulation was dependent on exposure concentration, $F(2, 44) = 34.2$, $p \leq 0.001$).

In order to evaluate translocation of the CdS-QDs or the dissolved Cd^{2+} ions to the aerial tissues, the stems and leaves were separately analyzed for Cd content (Fig. 3B, C). At 100 mg/L, no significant difference was seen in the stem or leaf Cd contents in CdS-QDs compared to bulk-CdS treatments. However, only stems from 100 mg/L QD-GLY exposed plants accumulated significantly higher amount of Cd than $CdCl_2$ and QD-MAA treatments. At 200 mg/L QD-PVP, the stems accumulated Cd at similar level as QD-GLY treatments (92 ± 16 μg/g DW), but the amount was significantly higher than QD-Bare (39 ± 4 μg/g DW), QD-TOPO (44 ± 12 μg/g DW), and QD-MAA (37 ± 5 μg/g DW). In the stems, there was no uniform dose-dependent trend in Cd accumulation for the CdS-QDs, except in QD-PVP, which at 200 mg/L accumulated 99 ± 16 μg Cd/g DW that was significantly higher ($p = 0.012$) than 50 mg/L treatment (32 ± 9 μg/g DW) (Fig. 3B). Similar to stems, only QD-PVP leaves showed a dose-dependent trend, although not statistically significant, with 1.5 ± 0.5, 3.2 ± 0.6, and 4.8 ± 1.2 μg Cd/g DW at 50, 100 and 200 mg/L QD-PVP, respectively.

For a more complete assessment of aerial translocation, we also calculated Cd accumulation in shoots (including stems and leaves) (Fig. S4). QD-PVP 200 mg/L plants accumulated the highest Cd levels in the shoots (73.7 ± 13.4 μg/g DW), and this level is significantly different from all treatments except QD-GLY. Due to strong auto-fluorescence of the plant tissues and fluorescence quenching of the QDs in the aqueous solution, it was not possible to track the QDs *in vivo* using confocal microscopy. Thus, definitive evidence could not be drawn to ascertain if the Cd inside the tissues was in the form of Cd^{2+} or QDs. Previous studies also reported background fluorescence from tissues of ryegrass (*Lolium perenne*), onion (*Allium cepa*), chrysanthemum (*Chrysanthemum* sp.) and *A. thaliana*, and concluded limited transport of glycine-, mercaptosuccinic acid-, cysteine-, and amine-conjugated CdSe/ZnS QDs in the vasculature of the plants grown in aqueous suspensions amended with the particles (Al-Salim et al., 2011). However, the study did not provide spectroscopic confirmation of the constituent elements of the QD in the vascular tissues, thus it is confounding to conclude if there was no transport or if only the fluorescence was quenched. As our study was intended for exploring the biological interactions with CdS-QDs, characterizing Cd speciation *in vivo* was out of the current scope.

3.5. Impact of surface coating on Cd bioavailability and translocation

The translocation factor of Cd in the soybean plants was calculated as C_{shoot}/C_{root}. Although the effective Cd concentration in the leaves from the $CdCl_2$ treatment was not significantly different from the bulk and 100 mg/L CdS-QD exposures, this treatment had a significantly higher translocation factor, TF (0.13 ± 0.03) compared to all CdS treatments at 100 mg/L (~0.03 to 0.05), except QD-GLY (0.08 ± 0.01), as shown in Table S2. As the Cd^{2+} from the $CdCl_2$ treatment was readily available to the plants, it was rapidly transported to the aerial tissues of the soybean plants. Compared to $CdCl_2$ treatment, higher levels of Cd in the CdS-QD roots but similar levels in leaves suggests that aerial translocation of Cd from the CdS-QDs may have been contributed from the Cd^{2+} release in the roots or during translocation. Although at 200 mg/L, the CdS-QD exposed roots accumulated more Cd than at 50 mg/L, the leaves and stems from either treatment levels accumulated similar amounts of the metal, except QD-PVP (Figs. 3, S4). This suggests that at higher CdS-QD treatments, the particles primarily sequestered in the root tissues. According to FTIR results, the attachment of PVP to CdS-QD core takes place *via* the O (Fig. 1), and thus the partial positive charge on the N results in an effective positive charge on the QD-PVP surface in aqueous suspension for 24 h (Fig. 2B). Thus, the positive charge on the QD-PVP may result in rapid attachment to the negatively-charged surface of the soybean roots, yielding more time for Cd^{2+} dissolution and subsequent translocation to aerial tissues. This also

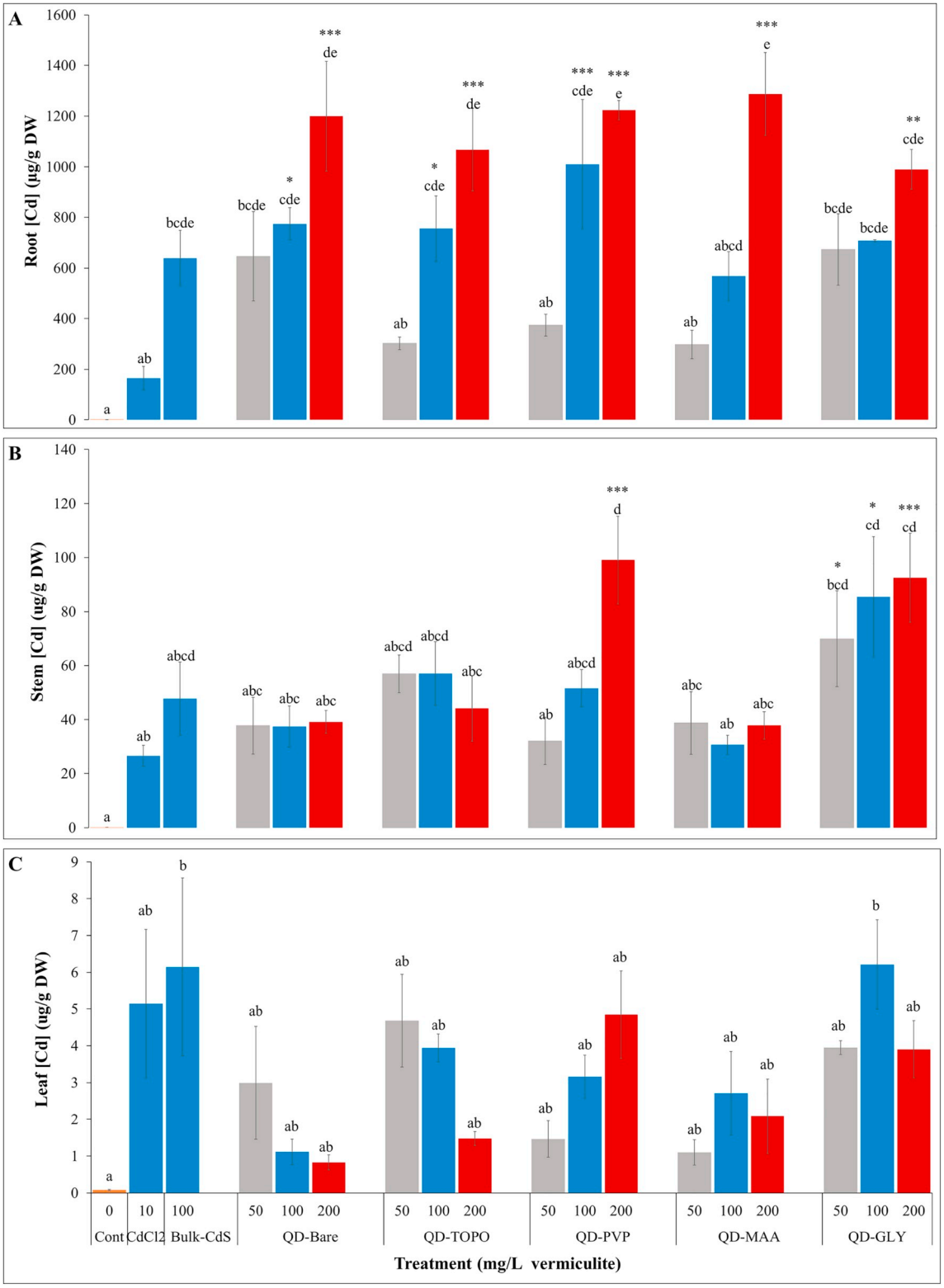

Fig. 3. Cadmium accumulation in (A) roots, (B) stems and (C) leaves of soybean plants exposed for 14 d to control, 50– 200 mg/L CdS-QDs, 100 mg/L bulk-CdS and 10 mg/L $CdCl_2$. Values are expressed as Mean ± SE. The bars with different letters represent significant difference as determined by one-way ANOVA and Tukey's multiple comparison test ($p \leq 0.05$). The bars with '*', '**', and '***' denote significant differences with respect to control at $p \leq 0.01$, ≤ 0.001, and ≤ 0.0001, respectively.

correlates with the reduction in leaf biomass in the 50 and 200 mg/L QD-PVP treatments (Fig. S2). A statistically significant interaction was noted between the effects of coating and concentration of CdS-QDs on Cd accumulation in shoots, $F(8,44) = 2.905$, $p = 0.011$. Simple main effects analysis showed that the exposure concentration significantly affected Cd accumulation in shoots only in QD-PVP treatments. Positively charged polyethyleneimine and neutrally charged amphiphilic polymer coating on CdSe/ZnS QDs were also reported to enhance Cd accumulation in *Daphnia*

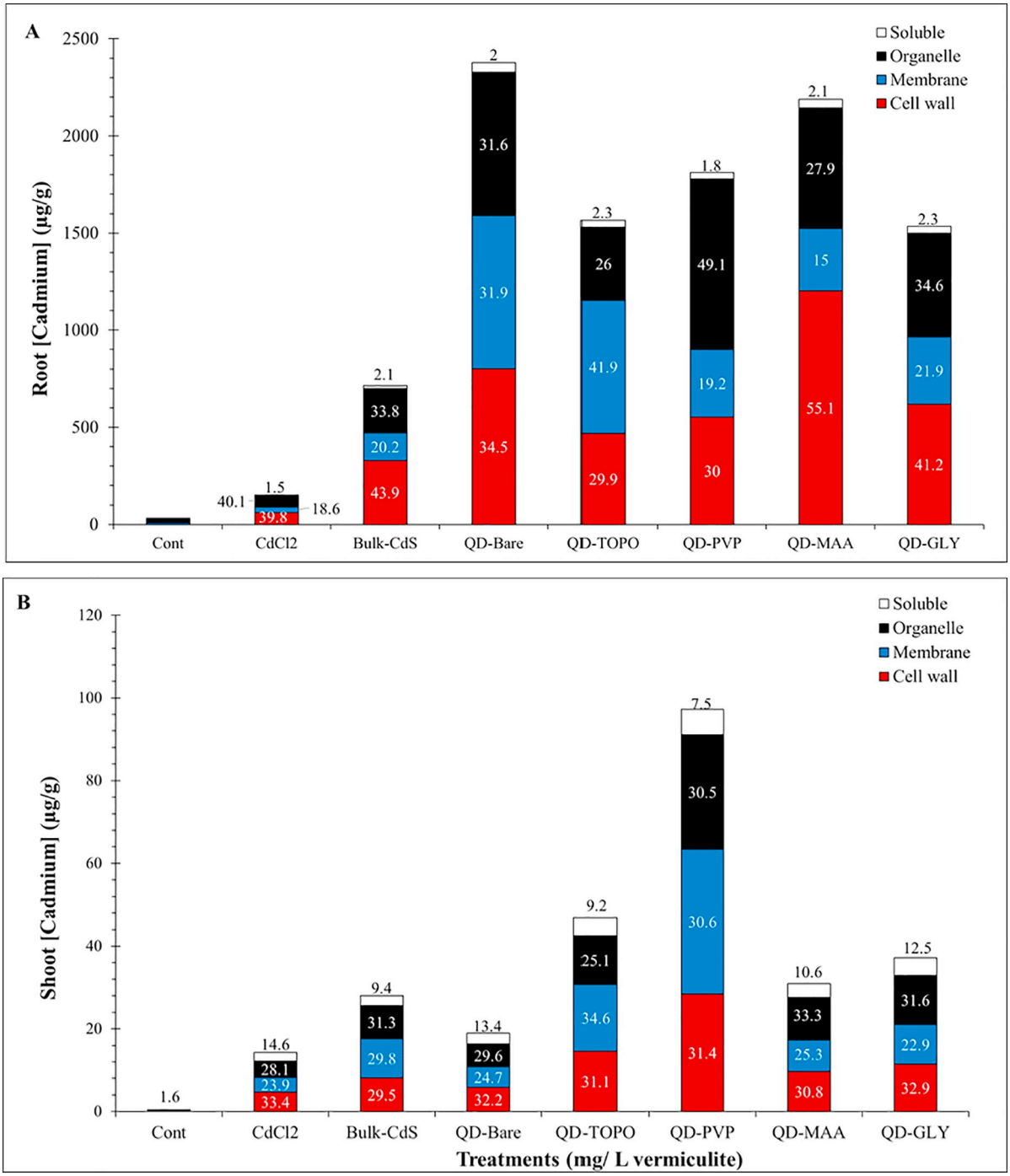

Fig. 4. Subcellular localization of Cd in (A) roots and (B) shoots of soybean plants exposed for 14 d to control, 200 mg/L CdS-QDs, 100 mg/L bulk-CdS and 10 mg/L $CdCl_2$. Values are expressed as mean in µg/g. The numbers on each segment of the bar represent the percent fraction of Cd in each compartment.

magna due to interaction with negatively charged cell membranes (Lee et al., 2016). Koo et al. showed that *A. thaliana* exposed to CdSe/CdZnS QD coated with positively charged polyethylenimine (PEI) containing secondary amines accumulated high concentrations of Cd in leaves. However, fluorescence imaging showed broad patches and aggregates as compared to a more homogeneous distribution in leaves that was reported with QD coated with positively charged poly(acrylic acid-ethylene glycol) (PAA-EG) (Koo et al., 2015). The authors suggested this difference was due to higher dissolution of Cd from PEI, resulting in greater availability and *in vivo* transport. Although QD-Bare also has a positive ζ-potential similar to QD-PVP (Fig. 2B), the linear increase in size of the aggregates (Fig. 2A) may restrict the entry into the root vascular system, and likely remain adhered to root surface. Although intact QD have been reported to transport inside plants, the stability of the particles *in vivo* is highly dependent on the surface coating (Koo et al., 2015). The QD-Bare and QD-TOPO treatments exhibited a decreasing trend in Cd accumulation in leaf tissues with increasing exposure concentration, although was statistically insignificant due to large variance. This supports the observed instability in aqueous media (Fig. 2) and probable aggregation at the nano-root interface.

In this study, all the treatments were conducted in a closed system in graduated centrifuge tubes; thus, it was possible to calculate a mass balance of Cd in the system (Fig. S5). The total mass of Cd added to each tube was: 0.244 mg for 10 mg/L $CdCl_2$ treatments, 3.12 mg for 100 mg/L bulk CdS treatments, and 1.56, 3.12 and 6.24 mg for 50, 100

and 200 mg/L CdS-QD treatments. The mass balance was calculated from the ICP-OES and ICP-MS values for Cd in vermiculite and plant tissues. The remaining fraction was attributed to the Cd fraction washed away during post-harvest cleaning with MQW and 0.1 M HNO_3. The mass balance shows that the major fraction of Cd in all the treatments remained in the vermiculite (57 to 81%), except QD-TOPO, where the sum of Cd content in vermiculite and plant tissues accounted for 42 to 49% of the total Cd supplied in the QD-TOPO treatments (Fig. S5). This was primarily due to the hydrophobic long alkyl chain on the surface of QD-TOPO (Fig. 1, Table S1), which remained loosely adhered in large aggregates to the roots surface. As shown in Fig. 1, QD-MAA was the most stable particle in aqueous suspensions for 14 d at 100 mg/L; however, due to limited dissolution (Fig. 2C) and high negative zeta potential (Fig. 2B), bioavailability was low and a significant fraction of the Cd was lost while rinsing the roots (Fig. S5). According to the mass balance calculations, the $CdCl_2$ was least retained on the root surface that was washed away (17% Cd) and was most sequestered (4% Cd) in the aerial tissues. Consequently, the total plant Cd fraction from $CdCl_2$ treatment was significantly higher than other CdS treatments (Fig. S5).

3.6. Cadmium subcellular localization in soybean roots and shoots

To investigate the cellular transport of the CdS-QDs in soybean plants, root and shoot tissues were fractionated by centrifugal separation into different cellular compartments, including the cell wall, membrane (plasma membrane, mitochondrial membrane, golgi membrane, endoplasmic reticulum membrane), intact large organelles (including mitochondria, peroxisome, lysosome, golgi apparatus, chloroplast) and soluble fraction containing vacuolar contents, cytoplasm, and the symplast. Each fraction was evaluated for Cd content per g fraction (DW) (Fig. 3). Unlike in aforementioned ICP-OES analysis where whole roots were acid rinsed with 0.01 M HNO_3 before digestion, for subcellular Cd quantification, the roots were lightly washed in MQW to minimize chemical damage to cell walls. Thus, this yielded higher total Cd concentration estimates in the roots (Fig. 4A) compared to acid rinsed samples (Fig. 3A). As noted in the methods section, samples had to be composited due to low mass and statistical analysis was not possible; however, the trends in the data are still instructive.

Roots from $CdCl_2$, bulk-CdS, QD-PVP, QD-MAA and QD-GLY treatments accumulated a major fraction of the Cd in the cell walls (40, 44, 30, 55, 41%, respectively) and organelle fraction (40, 34, 49, 28, 35%, respectively) (Fig. 4A). In several studies, fluorescence image tracking in plant tissues have suggested that the apoplastic pathway is the primary transport mechanism for nanomaterials in the plants (Koo et al., 2015; Hu et al., 2010). Fig. 4A clearly suggests that in the roots, Cd was transported to the stele primarily through the apoplast, due to its abundancy in cell wall of all the treatments. In QD-Bare, Cd distribution was equivalent in cell wall, cell membrane and organelle fractions (34, 32, 32%, respectively). Conversely, the largest fraction of Cd in QD-PVP roots was accumulated in the organelle fraction (49%). The sequestration of Cd in organelles in QD-PVP roots also suggests symplastic transport in this tissue. This also corroborates with higher Cd accumulation in aerial tissues of QD-PVP plants when compared to other treatments (Figs. 3B, 4B). Cadmium content in the soluble fraction of shoot cells increased in all the treatments, suggesting symplastic transport during loading of Cd into the vascular tissues (Song et al., 2017). Also, the vacuoles in the shoot tissues accumulated Cd, which decreased the load from the organelle fraction (Fig. 4B). This is a known heavy metal tolerance mechanism by plants upon exposure to high concentrations of these pollutants (Broadley et al., 2012). In all the treatments, approximately 2% Cd was accumulated in the soluble fraction of root cells (Fig. 4A); however, this value increased to 7 to 15% in the shoot cells, again suggesting symplastic transport in aerial tissues (Fig. 4B).

Interestingly, for QD-MAA exposed roots nearly 55% of the total accumulated Cd was restricted to the cell wall fraction (Fig. 4A). Djikanovic et al. showed that CdSe QDs binds to both cellulose and lignin in isolated cell walls (Djikanović et al., 2012). Hu et al. suggested apoplastic pathway as the major route of radial transport for water soluble MAA coated CdSe/ZnS QDs from the stele region of maize (*Zea mays*) (Hu et al., 2010). Due to high negative zeta potential of QD-MAA and relative high stability (Fig. 2), the particles were not as tightly bound to the negative charged carboxylic groups on the root surface when compared to other CdS-QDs. Also, the low dissolution of Cd^{2+} ions from the root surface restricts QD-MAA to the cell wall region (Fig. 4A). This also explains the lower Cd concentration in the shoots from QD-MAA treatment compared to QD-PVP (Fig. S6). Among all treatments, QD-TOPO roots had the greatest proportion of Cd (42%) attached to the membrane fractions, and only 26% was accumulated in the organelles (Fig. 3A). As QD-TOPO had the highest Cd^{2+} dissolution, the unstable large aggregates of these particles adheres to the root surface (Fig. S5) and the dissolved Cd^{2+} ions enter the symplast and are translocated to aerial tissues (Fig. 2C). It is possible that the QD-TOPO is immobilized on the plasma membrane due to the hydrophobic long alkyl chain and their affinity to phospholipid components of the membranes. Not surprisingly, the highest proportion of Cd in the shoot soluble fraction among all the exposures was reported in the $CdCl_2$ treatments.

3.7. Mineral acquisition and photosynthetic pigment accumulation

The CdS-QD treatments did not significantly alter the micro- and macronutrient acquisition by the soybean roots, although a decreasing trend was observed in all 200 mg/L QD treated roots with respect to control (Table S3). In contrast, all the nutrient elements in the roots showed a higher trend in the ionic treatment (10 mg/L $CdCl_2$). Root Mg and Fe in the plants exposed to 100, 200 mg/L QD-Bare, 200 mg/L QD-TOPO, 200 mg/L QD-GLY, and in all the treatment concentrations of QD-PVP and QD-MAA (50, 100, 200 mg/L) were significantly lower than the $CdCl_2$ treatment (Table S3 Root). Both Mg and Fe, critical for physiological and molecular processes in plants as component of chlorophyll and cofactors of associated proteins (Broadley et al., 2012), were not affected in the leaves from CdS-QD treatments (Table S3 Leaf). Biochemical analysis suggested that the CdS-QDs at 50 to 200 mg/L did not affect chlorophyll *a* formation and thus the light harvesting complexes and the photosystem reaction centers were not disturbed (Fig. S6). Carotene is an important photosynthetic pigment that helps plant to absorb the energy from the singlet oxygen that is produced during photosynthesis. At the applied treatment concentrations, carotene content as well as the ratio of chlorophyll *a/b* in the soybean leaves were unaffected by CdS-QD exposures (Fig. S6), and the different coatings had no observable impact on the photosynthetic process.

Compared to control, leaf Cu content was significantly decreased in all the 200 mg/L QD treatments (61, 51, 57, 53% in QD-Bare, QD-TOPO, QD-MAA and QD-GLY, respectively), except for QD-PVP, where the decrease was not statistically significant ($p = 0.475$; 35% decrease) (Table S3) content in the plants exposed to 10 mg/L $CdCl_2$, 100 mg/L bulk-CdS and lower levels of CdS-QDs (50 and 100 mg/L) was not altered. The uptake and translocation of Cd^{2+} in plants is driven by metal transporters from the natural resistance-associated macrophage protein (NRAMP) and zinc-regulated transporter/iron-regulated transporter-related protein (ZIP) families, both of which are present in the cell membrane (Hédiji et al., 2015; Yoneyama et al., 2015). These transporters also control the cellular transport of similar valence metal ions such as Fe^{2+}, Cu^{2+} as well as Zn^{2+}. Thus, competitive binding to the transporters possibly mediates the uptake of Cd and subsequently may limit the acquisition of these important micronutrients by the plants. The potential implications of this reduced micronutrient accumulation are not currently known. Hédiji et al. previously showed that 100 µM Cd treatment decreased Cu accumulation in the photosynthetic tissues of tomato (*Solanum lycopersicum*) (Hédiji et al., 2015). Copper is an essential micronutrient in the plants which is involved in the

photosynthetic process and disease resistance (Broadley et al., 2012). Thus, reduction in Cu content in response to QD exposure may affect soybean metabolic processes. Interestingly, although soybean leaves from QD-PVP treatment accumulated the most Cd in the tissues (Fig. 3C), the leaf Cu content in these plants was not significantly reduced, unlike the other QDs treatments. This again suggests that Cd^{2+} from QD-PVP or the particle itself possibly transport differently than the other particles in the soybean plants.

3.8. Effect of CdS-QDs on soybean metabolic processes

Although several studies have addressed the uptake and transport of different types of QDs in plants, there are no reports on the cellular response of the plants to these materials. As discussed in the previous section, most CdS-QDs were accumulated on the root cell walls and followed an apoplastic pathway; subsequently, a fraction was taken up as Cd^{2+} ions into the organelles and distributed and accumulated in aerial tissues of the plants. The surface coating on the CdS-QDs determined the dissolution and subcellular localization of Cd in the tissues, and hence, the resulting toxic response. It is well established that Cd^{2+} ions cause oxidative stress and may affect metabolic processes in plants (Mishra et al., 2006; Yang et al., 2012). Phenolic compounds are a group of secondary metabolites which play a major role in combating oxidative stress in plants. As shown in Fig. S7, the total phenolic content in the shoots of plants exposed to 10 mg/L $CdCl_2$, 100 mg/L bulk CdS and 50 to 200 mg/L CdS-QDs was not significantly affected.

The total soluble protein content (Fig. S8) and the activities of four antioxidant enzymes, including catalase (CAT), guaiacol peroxidase (GPX), ascorbate peroxidase (APX), and superoxide dismutase (SOD) (Fig. 5) were measured in the leaves of soybean plants exposed to CdS-QDs, $CdCl_2$, and bulk-CdS. SOD acts as the first line of defense during oxidative stress, reducing superoxide radicals to hydrogen peroxide, which are then further reduced to water and molecular oxygen by CAT and/or peroxidases, depending on the location of oxidative stress (Mishra et al., 2006). Different isoforms of SOD are specific to different organelles, including chloroplasts, mitochondria, peroxisomes, as well as to the cytosol and apoplast. CAT is present in mitochondria and peroxisomes, whereas APX functions in the chloroplast as part of the ascorbate-glutathione cycle. GPX is cell wall bound antioxidant enzyme and is also found in the cytoplasm (Mishra et al., 2006). QD-Bare, TOPO and PVP did not affect the enzymes of oxidative stress or the total protein content in the soybean leaves. However, in the leaves, the soluble protein content was increased significantly in 50 mg/L QD-GLY treatment ($p = 0.001$), (Fig. S8B) and the CAT activity was simultaneously reduced significantly at $p = 0.005$, with respect to control (Fig. 5). In the leaves from 100, and 200 mg/L QD-GLY treatment, there was a statistically insignificant increase ($p = 0.213$, and 0.317, respectively) in protein content; however CAT activities decreased significantly ($p = 0.005$ and 0.027, respectively) The reduced CAT activity in the QD-GLY leaves could be attributed to enzyme inactivation due to the significant oxidative stress from Cd accumulation in the shoot tissues (Figs. 3C, S4). Upon exposure to Cd (25 to 100 μM), the wetland macrophyte *Bacopa monnieri* exhibited reduced CAT activity in the leaves compared to control plants, but this was compensated for with higher activities of APX and GPX (Mishra et al., 2006). In our study, GPX activity showed an increasing trend in all the treatments but was significantly increased in the leaves of 100 mg/L QD-MAA and QD-GLY; in addition, 50 and 100 mg/L QD-MAA also significantly increased APX activity with respect to the control (Fig. 4). Thus, the oxidative stress in all the treatments appears to have been effectively quenched by the antioxidant enzymes, particularly peroxidases.

To investigate the reduction in secondary root hairs and browning of the roots in the QD treatments, (Fig. S3), the total lignin content was quantified in the roots. Compared to the control, the lignin content in all the Cd treatments were significantly affected, except at 50 mg/L QD-TOPO (Fig. 6). The lignin content was reduced in the roots from QD-Bare (50 mg/L), QD-TOPO (100 mg/L), and QD-PVP (50 and 200 mg/L) treated plants, but increased in $CdCl_2$, bulk-CdS, QD-Bare (100, 200 mg/L), QD-TOPO (200 mg/L), QD-PVP (100 mg/L) and all levels of QD-MAA and QD-GLY. The reduction in the lignin content in QD-PVP at 200 mg/L potentially explains the easy entry of the particle into the cells, thereby leading to higher Cd fraction in the organelles than the cell wall (Fig. 4A). QD-Bare roots at 200 mg/L had the highest lignin content (Fig. 6), which correlates with the significant reduction of secondary hair growth in the zone of maturation (Fig. S3). Cell wall thickening by lignification is a known protection strategy of plants against heavy metal exposure. In a cell culture suspension of *Medicago sativa*, mercaptopropanoic acid coated-CdSe/ZnS QDs were also shown to induce cell wall lignification and crosslinking of cell wall components (Santos et al., 2010).

Partial least square discriminant analysis (PLS-DA), a supervised multivariate dimensionality-reduction tool was used for the 18 amino acids analyzed using LC-MS to identify features in order to determine the separation between the treatment groups (Figs. 7A, S9). The PLS-DA score plot (Fig. 7A) clearly shows that at 100 mg/L treatment levels, QD-MAA and QD-GLY were separated from control, bulk CdS and $CdCl_2$ treatments. Using variable importance in projection (VIP) score, nine amino acids, including threonine (*Thr*), glycine (*Gly*), aspartic acid (*Asp*), tryptophan (*Trp*), valine (*Val*), citrulline (*Cit*), leucine (*Leu*), and phenylalanine (*Phe*), with VIP > 1 were identified as the responsible features for the separation (Fig. S9). As evident from the heat map representing the fold change in amino acid content in the leaves, 100 mg/L QD-GLY exposure resulted in significantly high level of *Glu* and *Met* ($p \leq 0.001$), compared to all 100 mg/L CdS-QD treatments, except QD-MAA (Fig. 7B). Based on the ICP-MS results, the shoots of QD-GLY accumulated the highest content of Cd (Fig. S4), reducing the CAT activity and increasing the peroxidase activity. In addition, *Gly* content did not increase in the QD-GLY leaves (Fig. 7), suggesting that the QD-GLY was translocated to aerial tissues as Cd^{2+} ions. However, QD-MAA at 100 mg/L accumulated *Phe* at significantly high level, compared to all treatments, except QD-GLY and QD-PVP (Fig. 6B). Proline (*Pro*) is an important amino acid which is considered as an indicator of stress in plants, and its role as molecular chaperone to maintain protein integrity and stress tolerance has been suggested (Hayat et al., 2012). It was significantly increased in the leaves from 100 mg/L QD-Bare exposed plants compared to other treatments, except QD-GLY and QD-TOPO. Under stress condition, *Pro* is reported to be biosynthesized using glutamate (*Glu*) pathway (Hayat et al., 2012). In the leaves from 100 mg/L QD-Bare, *Glu* content was also enhanced by 31% compared to control; although not statistically significant, it explains the increased response of *Pro*. At higher treatment level (200 mg/L), QD-Bare significantly increased thirteen amino acid content in the leaves at $p \leq 0.05$, specifically *Glu*, *Pro*, *Phe*, *Met*, *Thr*, *Asp*, *Gly*, *Cit*, asparagine (*Asn*), isoleucine (*Ile*), valine (*Val*), alanine (*Ala*), histidine (*His*), and lysine (*Lys*) (Fig. S10). This correlated with the highest fraction of Cd in the shoot soluble content in the 200 mg/L QD-Bare plants. The affected amino acids play a major role in amino acid and protein biosynthesis and other important metabolic processes. Phenylalanine participates as a substrate in the phenylpropanoid pathway, in which a wide range of secondary metabolites are produced including antioxidative metabolites (flavonoids, anthocyanins, lignins and phenylpropanoic acids including salicylic acid) and phenolic compounds (Zemanová et al., 2017). The increase in *Phe* in response to 200 mg/L QD-Bare supports the significant lignification observed in the root tissues (Fig. 6). Branched chain amino acids such as *Val*, *Leu* and *Ile* play a major role in balancing fluxes between amino acid pathways in order to maintain homeostasis (Zemanová et al., 2017). *Thr* and *Met* catabolism determines *Ile* availability as the metabolic pathways involving these three amino acids are intricately connected. The significant increase of amino acids in the leaves exposed to QD-Bare thus suggests increased production of antioxidative metabolites (Fig. 7). Although the ionic, bulk-CdS and 50 or 100 mg/L CdS-QDs did not affect the *Pro* content, the amounts were

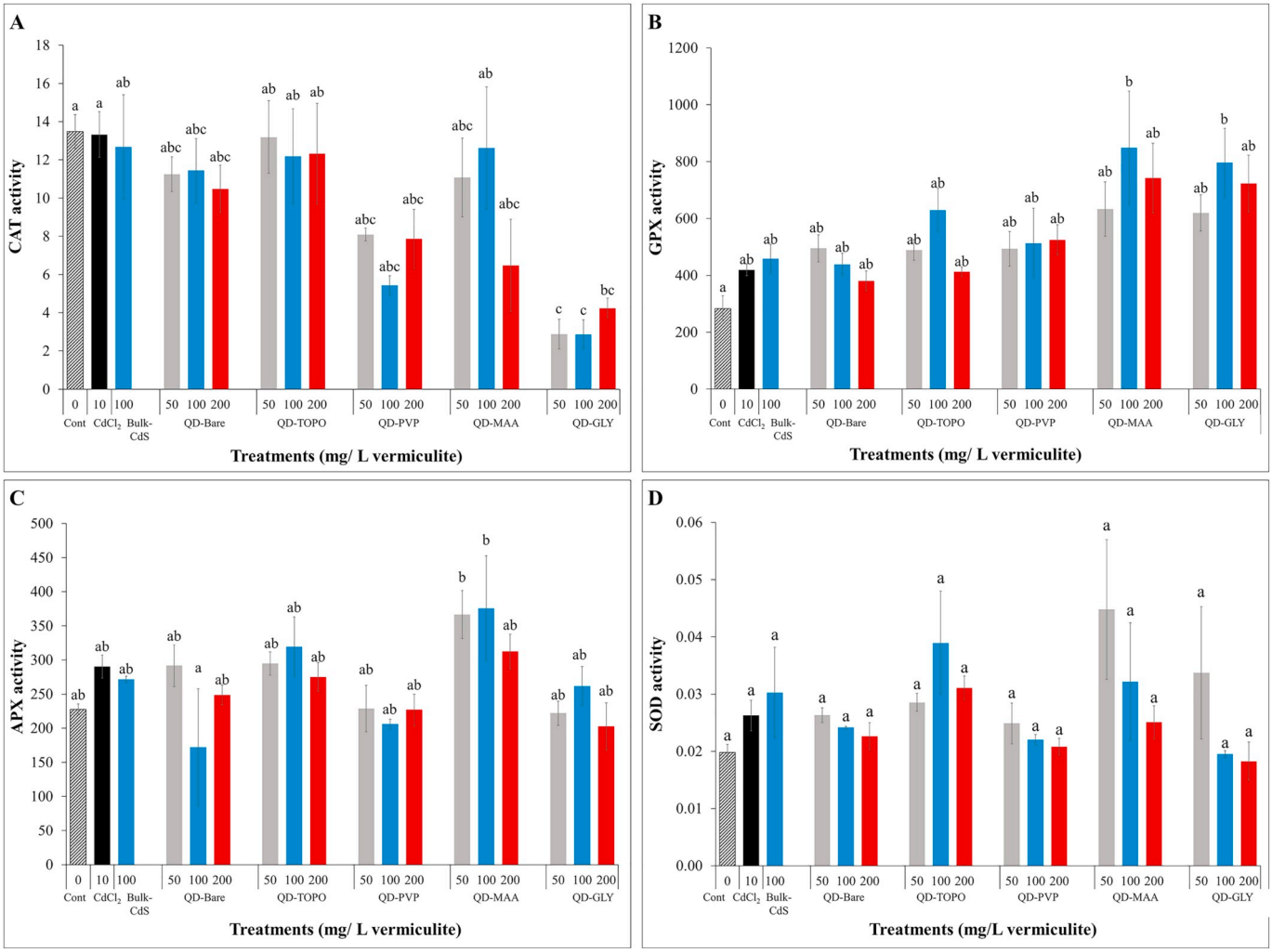

Fig. 5. Antioxidant enzyme activities in the leaves of soybean plants exposed for 14 d to control, 50–200 mg/L CdS-QDs, 100 mg/L bulk-CdS and 10 mg/L $CdCl_2$. (A) Catalase, CAT, (B) ascorbate peroxidase, APX, (C) guaiacol peroxidase, GPX activities, expressed as mg H_2O_2 degraded min^{-1} (mg protein)$^{-1}$, (D) superoxide dismutase, SOD activity expressed as Units (mg protein)$^{-1}$). Values are expressed as Mean ± SE. The bars with different letters represent significant differences as determined by one-way ANOVA and Tukey's multiple comparison test ($p \leq 0.05$).

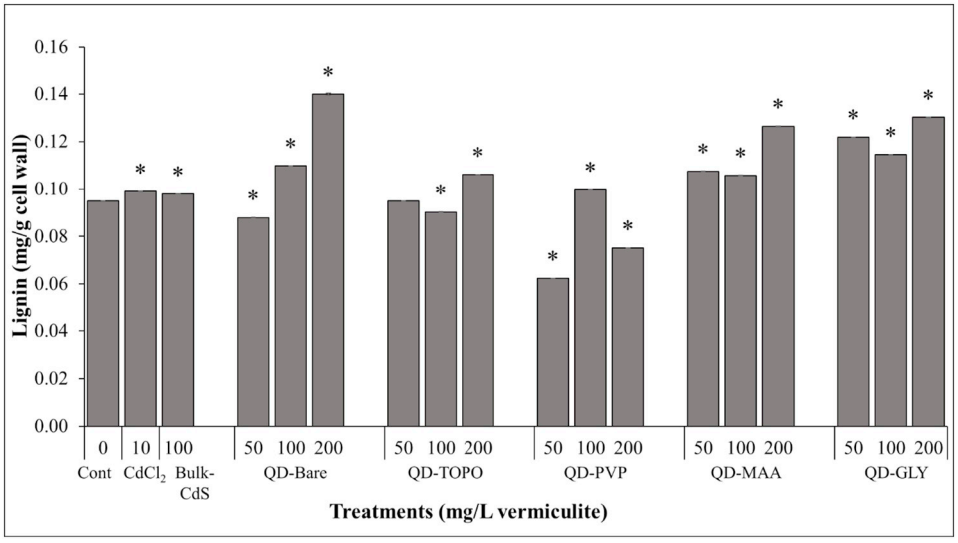

Fig. 6. Total lignin content (mg/g cell wall) in the roots of soybean plants exposed for 14 d to control, 50–200 mg/L synthesized CdS-QDs, 100 mg/L bulk-CdS and 10 mg/L $CdCl_2$. Values are expressed as Mean ± SE. The bars with '*' represent significant differences as determined by one-way ANOVA and Tukey's multiple comparison test ($p \leq 0.05$).

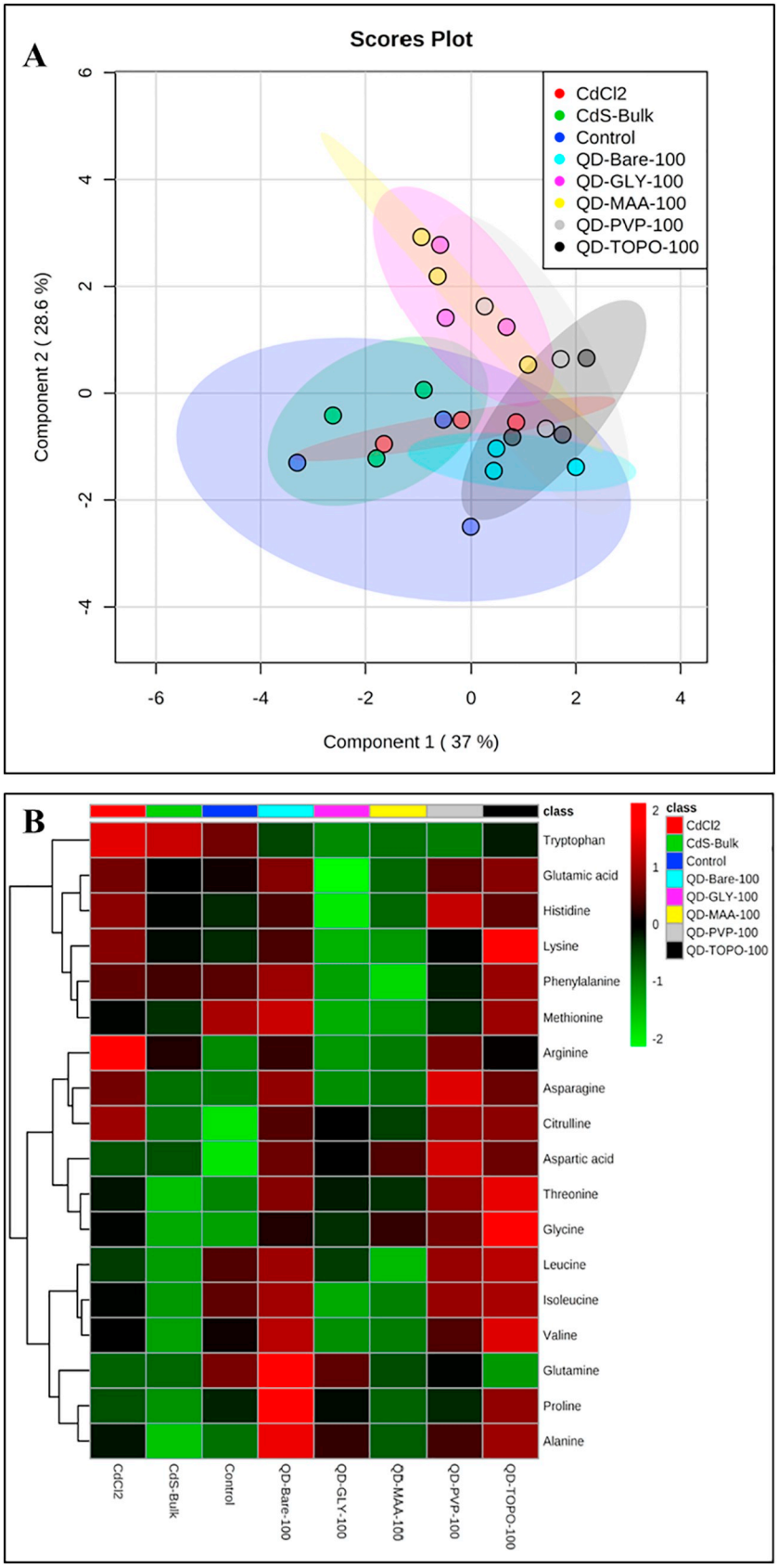

Fig. 7. Amino acid determination in the leaves of soybean plants exposed to control, 100 mg/L CdS-QDs, 100 mg/L bulk-CdS and 10 mg/L $CdCl_2$ treatments. (A) Partial least square discriminant analysis (PLS-DA) score plot of the amino acid contents. The color shaded area around each data point represent 95% confidence region. (B) Heat map illustrating normalized fold change of amino acid in the leaves. The rows displays the amino acids and the columns represent the samples. Red and green color indicate higher and lower amino acid content, respectively.

increased at all 200 mg/L QD treatments, although the effect was statistically significant only for QD-Bare and QD-MAA (Fig. S10). The CdS-QDs at 50 mg/L treatment and 10 mg/L $CdCl_2$ and 100 mg/L bulk-CdS did not significantly alter the amino acid contents in the leaves compared to control. Collectively, the results suggest that the amino acid metabolism in soybean leaves was affected when exposed to high concentration of QDs. Thus, it is clear that different surface coatings and concentration determined the regulation of metabolic processes in soybean plants.

4. Conclusions

This study clearly demonstrates that the fate and environmental behavior of the coated-ENMs depends on the exposed functional groups that determines the effective surface charge, polarity, dissolution, and affinity to biomolecules. The results imply that mercaptoacetic acid is an efficient stabilizer for CdS-QDs at least for two weeks in an aqueous suspension and limits dissolution of Cd^{2+} ions, resulting in low Cd translocation to aerial tissues of soybean plants. In contrary, CdS-QDs coated with trioctylphosphine oxide is highly unstable and aggregates instantly in suspension. It also releases maximum Cd^{2+} ions which accumulates in the cell membranes of plants. Coating CdS-QDs with polyvinylpyrrolidone-like molecules renders a positive surface charge allowing efficient transport of Cd to root cell organelles, with subsequent translocation to aerial tissues which results in decreased aerial biomass; however, the metabolic processes involved were unclear. The capping of CdS-QD with an amino acid, glycine, on the other hand negatively affects the plant metabolic processes. Thus, the study highlights that surface coatings play a definitive role in determining ENMs mode of uptake, bioaccumulation and differential biological response in plants. The findings hereby will be instrumental in the decision-making process of designing target specific ENMs for biological applications as well as assessing potential risk to plant health and associated food chain.

Acknowledgement

This study was supported by the U.S. Department of Agriculture (Hatch CONH00145 and CONH00147), U.S. Food and Drug Administration (FDA 1U18FD005505), National Science Foundation (NSF) and the U.S. Environmental Protection Agency (EPA) under NSF-EF0830117. Any opinions, findings, conclusions, or recommendations expressed in this material are those of the authors and do not necessarily reflect the views of the funding agencies. We thank the UCSB MRL Central Facilities for the use of their FTIR instrument. The UCSB MRL Central Facilities are supported by the MRSEC Program of the National Science Foundation under awards No. DMR 1121053; a member of the NSF-funded Materials Research Facilities Network (www.mrfn.org). NM and LP acknowledge the support of the project INTENSE, grant no. 652515.

Appendix A. Supplementary data

Supplementary data to this article can be found online at https://doi.org/10.1016/j.impact.2019.100151.

References

Abbasi, E., Kafshdooz, T., Bakhtiary, M., Nikzamir, N., Nikzamir, N., Nikzamir, M., Mohammadian, M., Akbarzadeh, A., 2016. Biomedical and biological applications of quantum dots. Artif. Cells Nanomed. Biotechnol. 44 (3), 885–891.

Al-Salim, N., Barraclough, E., Burgess, E., Clothier, B., Deurer, M., Green, S., Malone, L., Weir, G., 2011. Quantum dot transport in soil, plants, and insects. Sci. Total Environ. 409 (17), 3237–3248.

Altintas, Z., Davis, F., Scheller, F.W., 2017. Applications of Quantum Dots in Biosensors and Diagnostics. In: Altintas, Z. (Ed.), Biosensors and Nanotechnology, pp. 185–196.

Ashfaq, M., Verma, N., Khan, S., 2017. Carbon nanofibers as a micronutrient carrier in plants: efficient translocation and controlled release of Cu nanoparticles. Environ. Sci.: Nano 4 (1), 138–148.

Boles, M.A., Ling, D., Hyeon, T., Talapin, D.V., 2016. The surface science of nanocrystals. Nat. Mater. 15, 141.

Bradford, M.M., 1976. A rapid and sensitive method for the quantitation of microgram quantities of protein utilizing the principle of protein-dye binding. Anal. Biochem. 72 (1), 248–254.

Broadley, M., Brown, P., Cakmak, I., Rengel, Z., Zhao, F., 2012. Chapter 7 - function of nutrients: micronutrients. In: Marschner, P. (Ed.), Marschner's Mineral Nutrition of Higher Plants, third edition. Academic Press, San Diego, pp. 191–248.

Calestani, D., Villani, M., Mosca, R., Lazzarini, L., Coppedè, N., Dhanabalan, S.C., Zappettini, A., 2014. Selective response inversion to NO_2 and acetic acid in ZnO and CdS nanocomposite gas sensor. Nanotechnology 25 (36), 365502.

Djikanović, D., Kalauzi, A., Jeremić, M., Xu, J., Mićić, M., Whyte, J.D., Leblanc, R.M., Radotić, K., 2012. Interaction of the CdSe quantum dots with plant cell walls. Colloids Surf. B: Biointerfaces 91, 41–47.

Domingos, R.F., Tufenkji, N., Wilkinson, K.J., 2009. Aggregation of titanium dioxide nanoparticles: role of a fulvic acid. Environ. Sci. Technol. 43 (5), 1282–1286.

Domingos, R.F., Franco, C., Pinheiro, J.P., 2013. Stability of core/shell quantum dots—role of pH and small organic ligands. Environ. Sci. Pollut. Res. 20 (7), 4872–4880.

Efros, A.L., Delehanty, J.B., Huston, A.L., Medintz, I.L., Barbic, M., Harris, T.D., 2018. Evaluating the potential of using quantum dots for monitoring electrical signals in neurons. Nat. Nanotechnol. 13 (4), 278–288.

Finger-Teixeira, A., Lucio Ferrarese, M.D.L., Ricardo Soares, A., da Silva, D., Ferrarese-Filho, O., 2010. Cadmium-induced lignification restricts soybean root growth. Ecotoxicol. Environ. Saf. 73 (8), 1959–1964.

Fourati, E., Wali, M., Vogel-Mikuš, K., Abdelly, C., Ghnaya, T., 2016. Nickel tolerance, accumulation and subcellular distribution in the halophytes Sesuvium portulacastrum and Cakile maritima. Plant Physiol. Biochem. 108, 295–303.

Gaceur, M., Giraud, M., Hemadi, M., Nowak, S., Menguy, N., Quisefit, J.P., David, K., Jahanbin, T., Benderbous, S., Boissière, M., Ammar, S., 2012. Polyol-synthesized Zn0.9Mn0.1S nanoparticles as potential luminescent and magnetic bimodal imaging probes: synthesis, characterization, and toxicity study. J. Nanopart. Res. 14 (7), 932.

Garner, K.L., Suh, S., Keller, A.A., 2017. Assessing the risk of engineered nanomaterials in the environment: development and application of the nanoFate model. Environ. Sci. Technol. 51 (10), 5541–5551.

Green, M., 2010. The nature of quantum dot capping ligands. J. Mater. Chem. 20 (28), 5797–5809.

Gupta, G.S., Kumar, A., Senapati, V.A., Pandey, A.K., Shanker, R., Dhawan, A., 2017. Laboratory scale microbial food chain to study bioaccumulation, biomagnification, and ecotoxicity of cadmium telluride quantum dots. Environ. Sci. Technol. 51 (3), 1695–1706.

Hayat, S., Hayat, Q., Alyemeni, M.N., Wani, A.S., Pichtel, J., Ahmad, A., 2012. Role of proline under changing environments: a review. Plant Signal. Behav. 7 (11), 1456–1466.

Hédiji, H., Djebali, W., Belkadhi, A., Cabasson, C., Moing, A., Rolin, D., Brouquisse, R., Gallusci, P., Chaïbi, W., 2015. Impact of long-term cadmium exposure on mineral content of Solanum lycopersicum plants: consequences on fruit production. S. Afr. J. Bot. 97, 176–181.

Hernández, L.E., Lozano-Rodríguez, E., Gárate, A.n., Ramón, C.-R., 1998. Influence of cadmium on the uptake, tissue accumulation and subcellular distribution of manganese in pea seedlings. Plant Sci. 132 (2), 139–151.

Hu, Y., Li, J., Ma, L., Peng, Q., Feng, W., Zhang, L., He, S., Yang, F., Huang, J., Li, L., 2010. High efficiency transport of quantum dots into plant roots with the aid of silwet L-77. Plant Physiol. Biochem. 48 (8), 703–709.

Huang, Y., Li, W., Minakova, A.S., Anumol, T., Keller, A.A., 2018. Quantitative analysis of changes in amino acids levels for cucumber (Cucumis sativus) exposed to nano copper. NanoImpact 12, 9–17.

Javed, H., Fatima, K., Akhter, Z., Nadeem, M.A., Siddiq, M., Iqbal, A., 2016. Fluorescence modulation of cadmium sulfide quantum dots by azobenzene photochromic switches. Proceedings. Math. Phys. Eng. Sci. 472 (2186), 20150692 (-20150692).

Jin, S., Hu, Y., Gu, Z., Liu, L., Wu, H.-C., 2011. Application of quantum dots in biological imaging. J. Nanomater. 2011, 13.

Judy, J.D., Unrine, J.M., Rao, W., Wirick, S., Bertsch, P.M., 2012. Bioavailability of gold nanomaterials to plants: importance of particle size and surface coating. Environ. Sci. Technol. 46 (15), 8467–8474.

Koo, Y., Wang, J., Zhang, Q., Zhu, H., Chehab, E.W., Colvin, V.L., Alvarez, P.J.J., Braam, J., 2015. Fluorescence reports intact quantum dot uptake into roots and translocation to leaves of Arabidopsis thaliana and subsequent ingestion by insect herbivores. Environ. Sci. Technol. 49 (1), 626–632.

Kotkata, M.F., Masoud, A.E., Mohamed, M.B., Mahmoud, E.A., 2009. Synthesis and structural characterization of CdS nanoparticles. Physica E Low Dimens, Syst, Nanostruct. 41 (8), 1457–1465.

Lee, B.-T., Kim, H.-A., Williamson, J.L., Ranville, J.F., 2016. Bioaccumulation and in-vivo dissolution of CdSe/ZnS with three different surface coatings by Daphnia magna. Chemosphere 143, 115–122.

Li, H., Ye, X., Guo, X., Geng, Z., Wang, G., 2016. Effects of surface ligands on the uptake and transport of gold nanoparticles in rice and tomato. J. Hazard. Mater. 314, 188–196.

Li, R., Sun, H., Wang, S., Wang, Y., Yu, K., 2018. Retention of CdS/ZnS quantum dots (QDs) on the root epidermis of woody plant and its implications by benzo[a]pyrene: evidence from the in situ synchronous nanosecond time-resolved fluorescence spectra method. J. Agric. Food Chem. 66 (4), 814–821.

Luo, Y.-R., Kerr, J.A., 2018. Bond dissociation energies. In: Handbook of Chemistry and Physics, 87th online ed, (ed). http://www.hbcpnetbase.com/.

Majumdar, S., Peralta-Videa, J.R., Bandyopadhyay, S., Castillo-Michel, H., Hernandez-

Viezcas, J.-A., Sahi, S., Gardea-Torresdey, J.L., 2014. Exposure of cerium oxide nanoparticles to kidney bean shows disturbance in the plant defense mechanisms. J. Hazard. Mater. 278, 279–287.
Mishra, S., Srivastava, S., Tripathi, R.D., Govindarajan, R., Kuriakose, S.V., Prasad, M.N.V., 2006. Phytochelatin synthesis and response of antioxidants during cadmium stress in Bacopa monnieri L. Plant Physiol. Biochem. 44 (1), 25–37.
Mo, D., Hu, L., Zeng, G., Chen, G., Wan, J., Yu, Z., Huang, Z., He, K., Zhang, C., Cheng, M., 2017. Cadmium-containing quantum dots: properties, applications, and toxicity. Appl. Microbiol. Biotechnol. 101 (7), 2713–2733.
Moreira-Vilar, F.C., Siqueira-Soares, R.d.C., Finger-Teixeira, A., Oliveira, D.M.d., Ferro, A.P., da Rocha, G.J., Ferrarese, M.d.L.L., dos Santos, W.D., Ferrarese-Filho, O., 2014. The acetyl bromide method is faster, simpler and presents best recovery of lignin in different herbaceous tissues than Klason and thioglycolic acid methods. PLoS One 9 (10), e110000.
Mudunkotuwa, I.A., Grassian, V.H., 2015. Biological and environmental media control oxide nanoparticle surface composition: the roles of biological components (proteins and amino acids), inorganic oxyanions and humic acid. Environ. Sci.: Nano 2 (5), 429–439.
Ni, Z., Kim, E.D., Ha, M., Lackey, E., Liu, J., Zhang, Y., Sun, Q., Chen, Z.J., 2008. Altered circadian rhythms regulate growth vigour in hybrids and allopolyploids. Nature 457 (57227), 327–331.
Oh, E., Liu, R., Nel, A., Gemill, K.B., Bilal, M., Cohen, Y., Medintz, I.L., 2016. Meta-analysis of cellular toxicity for cadmium-containing quantum dots. Nat. Nanotechnol. 11, 479.
Owen, J., Brus, L., 2017. Chemical synthesis and luminescence applications of colloidal semiconductor quantum dots. J. Am. Chem. Soc. 139 (32), 10939–10943.
Petryayeva, E., Algar, W.R., Medintz, I.L., 2013. Quantum dots in bioanalysis: a review of applications across various platforms for fluorescence spectroscopy and imaging. Appl. Spectrosc. 67 (3), 215–252.
Rodrígues-Serrano, M., Romero-Puertas, MarÍA, C., Zabalza, A.N.A., Corpas Francisco, J., GÓMez, M., Del RÍO Luis, A., Sandalio Luisa, M., 2006. Cadmium effect on oxidative metabolism of pea (Pisum sativum L.) roots. Imaging of reactive oxygen species and nitric oxide accumulation in vivo. Plant Cell Environ. 29 (8), 1532–1544.
Ronzan, M., Piacentini, D., Fattorini, L., Della Rovere, F., Eiche, E., Riemann, M., Altamura, M.M., Falasca, G., 2018. Cadmium and arsenic affect root development in Oryza sativa L. negatively interacting with auxin. Environ. Exp. Bot. 151, 64–75.
Santos, A.R., Miguel, A.S., Tomaz, L., Malhó, R., Maycock, C., Vaz Patto, M.C., Fevereiro, P., Oliva, A., 2010. The impact of CdSe/ZnS quantum dots in cells of Medicago sativa in suspension culture. J. Nanobiotechnol. 8 (1), 24.
Shahi, A.K., Pandey, B.K., Singh, B.P., Gupta, B.K., Singh, S., Gopal, R., 2017. Photo physical studies of PVP arrested ZnS quantum dots. Electron. Mater. Lett. 13 (2), 160–167.
Shukla, N., Liu, C., Jones, P.M., Weller, D., 2003. FTIR study of surfactant bonding to FePt nanoparticles. J. Magn. Magn. Mater. 266 (1), 178–184.
Song, Y., Jin, L., Wang, X., 2017. Cadmium absorption and transportation pathways in plants. Int. J. Phytorem. 19 (2), 133–141.
Spielman-Sun, E., Lombi, E., Donner, E., Howard, D., Unrine, J.M., Lowry, G.V., 2017. Impact of surface charge on cerium oxide nanoparticle uptake and translocation by wheat (Triticum aestivum). Environ. Sci. Technol. 51 (13), 7361–7368.
Villani, M., Calestani, D., Lazzarini, L., Zanotti, L., Mosca, R., Zappettini, A., 2012. Extended functionality of ZnO nanotetrapods by solution-based coupling with CdS nanoparticles. J. Mater. Chem. 22 (12), 5694–5699.
Wang, Y., Nowack, B., 2018. Dynamic probabilistic material flow analysis of nano-SiO_2, nano iron oxides, nano-CeO_2, nano-Al_2O_3, and quantum dots in seven European regions. Environ. Pollut. 235, 589–601.
Wang, Y., Zhu, H., Becker, M.D., Englehart, J., Abriola, L.M., Colvin, V.L., Pennell, K.D., 2013. Effect of surface coating composition on quantum dot mobility in porous media. J. Nanopart. Res. 15 (8), 1805.
Whiteside, Matthew, D., Treseder, Kathleen, K., Atsatt, Peter, R., 2009. The brighter side of soils: quantum dots track organic nitrogen through fungi and plants. Ecology 90 (1), 100–108.
Xia, H., Wu, S., Su, X., Zhang, S., 2016. Monodisperse TiO_2 spheres with high charge density and their self-assembly. Chem. Asian J. 12 (1), 95–100.
Xie, B., Hu, R., Luo, X., 2016. Quantum dots-converted light-emitting diodes packaging for lighting and display: status and perspectives. J. Electron. Packag. 138 (2), 020803–020803-13.
Yang, S., Xie, J., Li, Q., 2012. Oxidative response and antioxidative mechanism in germinating soybean seeds exposed to cadmium. Int. J. Environ. Res. Public Health 9 (8), 2827–2838.
Yoneyama, T., Ishikawa, S., Fujimaki, S., 2015. Route and regulation of zinc, cadmium, and iron transport in rice plants (Oryza sativa L.) during vegetative growth and grain filling: metal transporters, metal speciation, grain cd reduction and Zn and Fe biofortification. Int. J. Mol. Sci. 16 (8).
Young, A.G., Green, D.P., McQuillan, A.J., 2006. Infrared spectroscopic studies of monothiol ligand adsorption on CdS nanocrystal films in aqueous solutions. Langmuir 22 (26), 11106–11112.
Young, A.G., Al-Salim, N., Green, D.P., McQuillan, A.J., 2008. Attenuated total reflection infrared studies of oleate and trioctylphosphine oxide ligand adsorption and exchange reactions on CdS quantum dot films. Langmuir 24 (8), 3841–3849.
Zemanová, V., Pavlík, M., Pavlíková, D., 2017. Cadmium toxicity induced contrasting patterns of concentrations of free sarcosine, specific amino acids and selected microelements in two Noccaea species. PLoS One 12 (5), e0177963.
Zhang, W., Schwab, A.P., White, J.C., Ma, X., 2018. Impact of nanoparticle surface properties on the attachment of cerium oxide nanoparticles to sand and kaolin. J. Environ. Qual. 47 (1), 129–138.
Zheng, W., Wang, S.Y., 2001. Antioxidant activity and phenolic compounds in selected herbs. J. Agric. Food Chem. 49 (11), 5165–5170.
Zhu, Z.-J., Wang, H., Yan, B., Zheng, H., Jiang, Y., Miranda, O.R., Rotello, V.M., Xing, B., Vachet, R.W., 2012. Effect of surface charge on the uptake and distribution of gold nanoparticles in four plant species. Environ. Sci. Technol. 46 (22), 12391–12398.